Authors
Kok-Hon Chew
Kang Tai
E.Y.K. Ng
Michael Muskulus

NTNU
Norwegian University of Science and Technology
Department of Civil and Transport Engineering
Report No.: BAT/MB/OW-R01/2015

OPTIMIZATION OF OFFSHORE WIND TURBINE SUPPORT STRUCTURES USING ANALYTICAL GRADIENT-BASED METHOD

18 March 2015, Trondheim, Norway

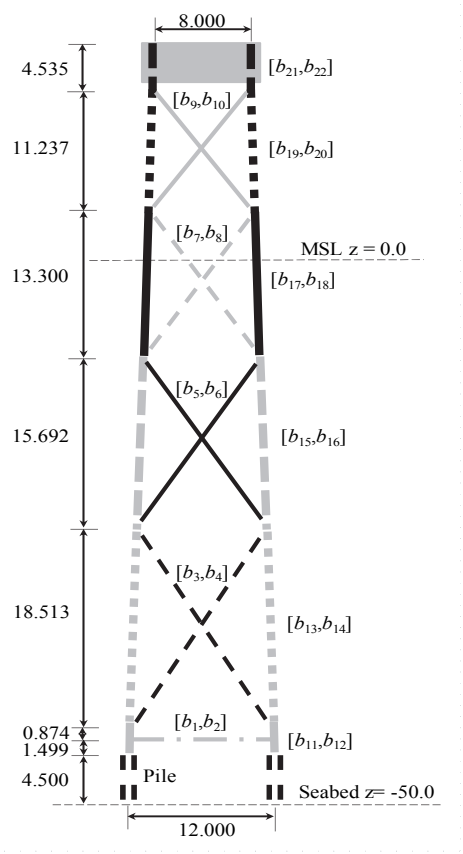

NTNU

REPORT DOCUMENTATION PAGE

NTNU
Department of Civil and Transport Engineering

Offshore wind technology group
Department of Civil and Transport Engineering
Norwegian University of Science and Technology

7491 Trondheim
Norway

REPORT NUMBER
BAT/MB/OW-R01/2015

ACCESSIBILITY
☒ PUBLIC
☐ INTERNAL
☐ CONFIDENTIAL

STATUS
☐ REVISION
☒ FINAL REPORT
☐ REVIEW / COMMENT
☐ DRAFT

TITLE
Optimization of Offshore Wind Turbine Support Structures Using Analytical Gradient-Based Method

DATE
18.03.2015

AUTHOR(S)
Kok-Hon Chew[1,2], Kang Tai[2], E.Y.K. Ng[2], Michael Muskulus[1]

[1]Department of Civil and Transport Engineering, NTNU, Trondheim, Norway
[2]School of Mechanical and Aerospace Engineering, Nanyang Technological University, Singapore

NO. OF PAGES
23

PROJECT CLIENT / SPONSOR
Research Council of Norway

PROJECT NAME
NOWITECH FME

FUNDING NUMBERS
193823

SUPERVISOR
M. Muskulus

SUMMARY

Design optimization of the offshore wind turbine support structure is an expensive task; due to the highly-constrained, non-convex and non-linear nature of the design problem. This report presents an analytical gradient-based method to solve this problem in an efficient and effective way. The design sensitivities of the objective and constraint functions are evaluated analytically while the optimization of the structure is performed, subject to sizing, eigenfrequency, extreme load and fatigue load constraints. A case study is carried out for the OC4 jacket substructure to evaluate the method. Results shows that an optimal jacket design with 52 percent structural mass reduction is attained in 27 iterations, while satisfying all design constraints under the simplified load cases used. Besides, it is shown that the analytical sensitivity analysis is more accurate and efficient than the often used finite difference approximations. It can avoid numerical artifacts that typically occur in the analysis of extreme load constraint sensitivities.

KEYWORDS
Structural optimization; sensitivity analysis; gradient-based; offshore wind; support structures.

APPROVED
Michael Muskulus

ARCHIVING
☒ Permanent link (DiVA) ☐ Group webpage ☐ Internal

Contents

1. Introduction

The support structure system typically contributes around 17 percent of the total capital cost in an offshore wind project [1]. It is an area which attracts numerous studies in academia and industry, due to the potential for cost reduction. Despite that structural optimization is heavily used in the automotive and aerospace industries; its implementation in offshore wind turbine structure design is comparably limited. Previous studies have suggested that the designs of various types of offshore wind turbine support structures, e.g. monopile, jacket, full-height lattice tower and spar-type floater, etc., can attain cost saving by using different simulation-based optimization approaches [2,3,4,5]. However, the design process often involves a large number of iterations since the optimization problem is highly constrained and non-convex [6]. Furthermore, the dynamic analysis of offshore wind system is prescribed to be carried out in time domain simulation in order to capture nonlinearities and time-history dependence, thus resulting in high computational demand [7]. As for the sensitivity analysis, finite difference method is normally employed to handle the complicated gradient calculation. Although the method is easy to implement, it suffers from computational inefficiency and possible numerical errors [8]. As a result, these bring the focus to research on an optimization methodology which is effective and efficient in designing the offshore wind turbine support structure, particularly for complex structure that has many design variables, e.g. space frame structure.

This report presents a dynamic response constrained optimization framework that is based on the gradient search method. The dynamic analysis is performed in time domain whilst the sensitivity analysis is conducted using analytical direct differentiation method (DDM). The scope of design constraints covers sizing, natural frequency, extreme load and fatigue load compliances. A case study on the jacket substructure of the Offshore Code Comparison Collaboration Continuation (OC4) Project – Phase I is also included in this study.

2. Optimal Design Problem Formulation

The dynamic response optimization problem of an offshore wind turbine support structure can be illustrated using the following general expression [9]:

$$\text{Find } \mathbf{b} \tag{1a}$$

$$\text{to minimize } f(\mathbf{b}) \tag{1b}$$

$$\text{subject to } g_i\left(\mathbf{b}, \mathbf{z}(t_j), \dot{\mathbf{z}}(t_j), \ddot{\mathbf{z}}(t_j), t_j\right) \le 0,\ i = 1,\ldots,p,\ j = 1,\ldots,q \tag{1c}$$

$$\text{and } \mathbf{M}\ddot{\mathbf{z}}(t_j) + \mathbf{C}\dot{\mathbf{z}}(t_j) + \mathbf{K}\mathbf{z}(t_j) - \mathbf{f}(t_j) = 0,\ j = 1,\ldots,q \tag{1d}$$

where f = objective function; g_i = constraint function; $\mathbf{b}$ = design variable vector; $\mathbf{z}(t_j), \dot{\mathbf{z}}(t_j)$ and $\ddot{\mathbf{z}}(t_j)$ = displacement, velocity and acceleration vectors, respectively; t_j = j th time step; $\mathbf{M}$, $\mathbf{C}$ and $\mathbf{K}$ = mass, damping and stiffness matrices, respectively; $\mathbf{f}(t_j)$ = force vector; p = number of constraints; and q = number of time steps.

2.1. Objective Function

The objective function to be minimized in this study is the mass of support structure [kg]. While the support structure is modelled using simple beam elements, the mass can be formulated as:

$$f = \sum_{n=1}^{N} \rho A_n L_n \text{ where } A_n = \pi(D_n t_n - t_n^2) \tag{2}$$

where ρ = material density [kg/m^3]; A_n = cross-sectional area [m^2]; L_n = length [m]; D_n = outer diameter [m]; and t_n = thickness of member [m].

2.2. Design Constraints

The design constraints are based on limit state functions as prescribed by the design standards and recommended practices used within the offshore and wind industries [7,10,11].

2.2.1. Sizing Constraints

Sizing constraints define the lower and upper bounds of the continuous design variables as well as the geometrical relationships among the variables, e.g. D_n/t_n, D_{brace}/D_{leg} and t_{brace}/t_{leg}.

$$g_1 = \mathbf{b}_{\min} \le \mathbf{b} \le \mathbf{b}_{\max} \tag{3}$$

$$g_2 = \mathbf{A}_{ineq}\mathbf{b} - \mathbf{c}_{ineq} \le 0 \tag{4}$$

where $\mathbf{b}_{\min}$ = lower bound; $\mathbf{b}_{\max}$ = upper bound; $\mathbf{A}_{ineq}$ and $\mathbf{c}_{ineq}$ = linear inequality constraint matrix and vector which define the geometrical relationships.

2.2.2. Natural Frequency Constraint

The natural frequencies of the overall wind turbine system ought to be assessed if they fall under the wave and wind (including the rotor rotational 1P and blade passing 3P) excitation frequency zones so as to avoid resonance [12]. While the design principle of a bottom fixed support structure is to withstand external excitation via structural resistance, the first mode natural frequencies are intended to lie in the soft-stiff region, as bounded in Eq. (5) [13]:

$$g_3 = 0.222 \text{ Hz} \le f_1 \le 0.311 \text{ Hz} \tag{5}$$

where f_1 = first mode natural frequencies [Hz].

2.2.3. Extreme Load Constraints

Ultimate limit state (ULS) analysis is performed on the offshore structure to evaluate if the tubular members and joints satisfy structural strength and stability requirements, i.e. yield check and buckling assessment. In this study, the extreme load constraints are formulated in accordance to ultimate limit state functions described in the NORSOK standard [10].

Under the complicated environmental conditions, the offshore tubular members are potentially subject to any combination of axial tension, axial compression, bending, shear and hydrostatic loads. The standard distinguishes members which are free from hydrostatic pressure, for instance the beams situated above the mean sea level (MSL) or flooded internally, see Eq. (6)-(10); and submerged members which experience hydrostatic pressure externally, see Eq. (11)-(15).

- Combined axial tension and bending:

$$g_{4a} = \left(N_{t,Sd}/N_{t,Rd}\right)^{1.75} + \left(M_{y,Sd}^2 + M_{z,Sd}^2\right)^{0.5} \Big/ M_{Rd} - 1.0 \le 0 \tag{6}$$

- Combined axial compression and bending; where the column buckling effect is included in Eq. (7):

$$g_{5a} = N_{c,Sd}/N_{c,Rd} + \left\{\left[C_{my}M_{y,Sd}/\left(1 - N_{c,Sd}/N_{Ey}\right)\right]^2 + \left[C_{mz}M_{z,Sd}/\left(1 - N_{c,Sd}/N_{Ez}\right)\right]^2\right\}^{0.5} \Big/ M_{Rd} - 1.0 \le 0 \tag{7}$$

$$g_{6a} = N_{c,Sd}/N_{cl,Rd} + \left(M_{y,Sd}^2 + M_{z,Sd}^2\right)^{0.5} \Big/ M_{Rd} - 1.0 \le 0 \tag{8}$$

- Interaction of shear, bending moment and torsional moment:

$$g_{8a} = M_{Sd} \Big/ \left[M_{Red,Rd}\left(1.4 - V_{Sd}/V_{Rd}\right)^{0.5}\right] - 1.0 \le 0 \text{ for } V_{Sd}/V_{Rd} \ge 0.4 \tag{9}$$

$$g_{8b} = M_{Sd}/M_{Red,Rd} - 1.0 \le 0 \text{ for } V_{Sd}/V_{Rd} < 0.4 \tag{10}$$

- Hoop buckling:

$$g_9 = \sigma_{p,Sd}/f_{h,Rd} - 1.0 \le 0 \tag{11}$$

- Combined axial tension, bending and hydrostatic pressure:

$$g_{4b} = \sigma_{at,Sd}/f_{th,Rd} + \left(\sigma_{my,Sd}^2 + \sigma_{mz,Sd}^2\right)^{0.5} \Big/ f_{mh,Rd} - 1.0 < 0 \tag{12}$$

- Combined axial compression, bending and hydrostatic pressure; where the column buckling effect is included in Eq. (13):

$$g_{5b} = \frac{\sigma_{ac,Sd} - \sigma_{q,Sd}}{f_{ch,Rd}} + \frac{1}{f_{mh,Rd}}\left\{\left[\frac{C_{my}\sigma_{my,Sd}}{1 - \left(\sigma_{ac,Sd} - \sigma_{q,Sd}\right)/f_{Ey}}\right]^2 + \left[\frac{C_{mz}\sigma_{mz,Sd}}{1 - \left(\sigma_{ac,Sd} - \sigma_{q,Sd}\right)/f_{Ez}}\right]^2\right\}^{0.5} - 1.0 \le 0 \tag{13}$$

$$g_{6b} = \sigma_{ac,Sd}/f_{cl,Rd} + \left(\sigma_{my,Sd}^2 + \sigma_{mz,Sd}^2\right)^{0.5} \Big/ f_{mh,Rd} - 1.0 \le 0 \tag{14}$$

$$g_7 = \left(\sigma_{c,Sd} - 0.5 f_{he}/\gamma_m\right)\Big/\left(f_{cle}/\gamma_m - 0.5 f_{he}/\gamma_m\right) + \left(\sigma_{p,Sd}\gamma_m/f_{he}\right)^2 - 1.0 \le 0 \tag{15}$$

where $N_{t,Sd}(\sigma_{at,Sd})$, $N_{c,Sd}(\sigma_{ac,Sd})$, $M_{y,Sd}(\sigma_{my,Sd})$, $M_{z,Sd}(\sigma_{mz,Sd})$ and V_{Sd} = design axial tensile force [N], compressive force [N], bending moments [Nm] about member y-axis (in-plane) and z-axis (out-of-plane) and shear force [N], respectively; $N_{t,Rd}(f_{th,Rd})$, $N_{c,Rd}(f_{ch,Rd})$, $N_{cl,Rd}(f_{cl,Rd})$, $N_{Ey}(f_{Ey})$, $N_{Ez}(f_{Ez})$, $M_{Rd}(f_{mh,Rd})$ and V_{Rd} = design resistances for axial tension [N], axial compression [N], local buckling [N], Euler buckling (member y- and z- axes) [N], bending [Nm] and shear [N], respectively; $\sigma_{p,Sd}$, $\sigma_{q,Sd}$

and $\sigma_{c,Sd}$ = design hoop stress, capped-end compression stress and maximum combined compression stress, respectively; and f_h, f_{he}, f_{cle}, C_{my}, C_{mz} and γ_m = design hoop buckling strength, elastic hoop buckling strength, characteristic elastic local buckling strength, reduction factors (member y- and z-axes) and partial safety factor for material, respectively. The symbols in parentheses refer to the corresponding stress terms. All stress units are in Pa.

Similarly, the resistances of tubular joints N_{Rdj}, $M_{y,Rdj}$ and $M_{z,Rdj}$ are checked to conform to the interaction equation for combined axial force and bending moments in the braces, see Eq. (16). The characteristic resistances depend on strength factor Q_u and chord action factor Q_f, which vary with respect to the joint configuration (i.e. joint type and joint dimension), material strength, as well as the presence of factored actions within the chords.

$$g_{10} = N_{Sd} \big/ N_{Rdj} + \left(M_{y,Sd} \big/ M_{y,Rdj} \right)^2 + M_{z,Sd} \big/ M_{z,Rdj} - 1.0 \le 0 \tag{16}$$

Since the extreme load constraints are time-dependent, they are required to be satisfied at all time-steps. Several methods are available to handle this type of constraint, and the worst case approach was implemented in this study. The method identifies the maximum violated limit state values in time as design constraints; while gradients are calculated for the constraints at those active time grid points.

2.2.4. Fatigue Load Constraint

Fatigue failure mode which often occurs at the tubular joints is another important aspect to be studied during the offshore structure design process. Typically, fatigue limit state (FLS) analysis is carried out on every tubular joint to ensure a minimum survivability of 20 years design lifetime. According to the DNV Recommended Practices C203, eight hot spot stresses (HSS) around the circumferential of intersection are determined from the superposition of nominal stresses that are pre-multiplied by stress concentration factors (SCF) [11]. The SCFs are calculated using empirical formulae, based on the joint configuration. After-which, the rainflow counting is performed to determine the effective number of stress cycles and the corresponding stress ranges [14]. The total equivalent damage is estimated using Palmgren-Miner's rule. The unity check of fatigue constraint is written as:

$$g_{11} = \sum_{i=1}^{I} \frac{1}{\bar{a}\eta} \left(\frac{t}{t_{ref}} \right)^{mk} n_i \left(\Delta\sigma_{i,HSS} \right)^m - 1.0 \le 0 \tag{17}$$

where $\bar{a}$ = intercept of S-N curve with log N axis; m = negative inverse slope of the S-N curve; $\Delta\sigma_{i,HSS}$ = constant stress range block of HSS [MPa]; n_i = number of stress cycles in stress block i; η = usage factor; t, t_{ref} and k = member thickness [m], reference thickness [m] and thickness exponent, respectively.

3. Integrated Optimization Framework

An integrated dynamic simulation and structural optimization tool was developed in Matlab to solve the constrained nonlinear programming (NLP) problem of offshore wind turbine support structure. The framework is as shown in Fig. 1. Iterative optimization procedures were carried out within the framework until the optimization task was complete.

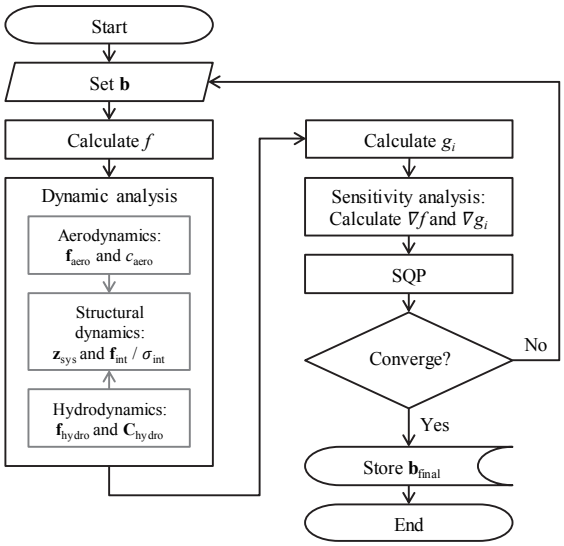

Fig. 1 Flowchart illustrating the integrated design optimization framework

3.1. Structural Dynamics

For simplification purpose, the Matlab code assumed a linear hydro-elastic offshore wind turbine (OWT) model with the aero-servo effects implemented as decoupled model [15]. The overall OWT system which comprises rotor-nacelle assembly (RNA) and support structure was modelled using three-dimensional Euler-Bernoulli beam elements. As for the RNA, the mechanical properties were based on the National Renewable Energy Laboratory (NREL) 5 MW reference turbine as defined in [16]. The inclusion of RNA within the OWT model captured the system eigen-modes accurately for dynamic analysis. Moreover, Rayleigh damping was incorporated as structural damping while Newmark-beta integration method was used to solve the dynamic governing equation [17].

3.2. Aerodynamic Loads

The aerodynamic force on the rotor was calculated using FEDEM WindPower Version R7.0.4[1] developed by FEDEM Technology AS, Trondheim. Its aerodynamic module is based on Aerodyn which supports full Blade Element Momentum (BEM) or Generalized Dynamic Wake (GDW) methods that account for tip or hub loss corrections [18]. The forces and moments in six degrees of freedom experienced at the hub node were then extracted into the Matlab model, as the external force vector $\mathbf{f}_{aero}$. In addition, the linear aerodynamic damping ratio ξ_{aero} was estimated by analysing the free decay vibration of the tower top motion, upon exerting a pulse loading on the turbine subject to the turbulent wind field, as described in [19,20]. The aerodynamic damping c_{aero} was then added into the **C** matrix in Eq. (1d).

[1] http://www.fedem.com/

3.3. Hydrostatic and Hydrodynamic Loads

The submerged parts of the substructure experience hydrostatic and hydrodynamic forces. Buoyancy was computed as the weight of the displaced liquid. In the case of flooded members, additional enclosed liquid mass was included. Both buoyancy and internal mass were summed up to the mean sea level (MSL). Additionally, the code could also account for marine growth mass. As for the hydrodynamic load, empirical Morison formula was used. The inertia force depends on both water particle acceleration and structural acceleration, whereby the latter term was shifted to the $\mathbf{M}$ matrix in Eq. (1d). Similarly, the quadratic drag force could be expanded into $\mathbf{C}_{hydro}(\mathbf{v}_w)\dot{\mathbf{z}}+\mathbf{f}_{hydro}(\mathbf{v}_w)$, where $\mathbf{C}_{hydro}(\mathbf{v}_w)$ = hydrodynamic damping matrix, assuming that $\dot{\mathbf{z}} \ll \mathbf{v}_w$. Then, the $\mathbf{C}_{hydro}$ was moved to the $\mathbf{C}$ matrix while $\mathbf{f}_{hydro}$ was retained as the external load in Eq. (1d).

3.4. Sensitivity Analysis

Design sensitivity analysis is a process that calculates the rate of performance measure change with respect to the design variables [21]. The performance measures here refer to the objective and constraint functions. The rate of change or simply gradient is required by the optimizer to determine the best direction for improvement during the optimization process. In this study, the gradient vectors were calculated using the DDM, as

$$\nabla f = \frac{\partial f}{\partial \mathbf{b}} \tag{18}$$

$$\nabla g_i = \frac{\partial g_i}{\partial \mathbf{b}} + \frac{\partial g_i}{\partial \mathbf{z}} \frac{\mathrm{d}\,\mathbf{z}}{\mathrm{d}\,\mathbf{b}} \tag{19}$$

where ∇f = gradient of objective function and ∇g_i = gradient of constraint function i.

The calculation of ∇f and ∇g_i for the sizing constraints are straightforward. As for the extreme load constraints, the ∇g_i can be treated in two parts. Firstly, $\mathrm{d}\mathbf{z}/\mathrm{d}\mathbf{b}$ in Eq. (19) could be summed up from $\mathrm{d}\mathbf{z}_{sta}/\mathrm{d}\mathbf{b}$ and $\mathrm{d}\mathbf{z}_{dyn}/\mathrm{d}\mathbf{b}$, i.e. derivatives of static and dynamic displacements. Both derivatives were solved using Eq. (20) and (21), respectively. The latter is a second order differential equation obtained when differentiating Eq. (1d) with respect to $\mathbf{b}$.

$$\frac{\mathrm{d}\mathbf{z}_{sta}}{\mathrm{d}\mathbf{b}} = \mathbf{K}^{-1}\left(\frac{\mathrm{d}\mathbf{f}_{sta}}{\mathrm{d}\mathbf{b}} - \frac{\mathrm{d}\mathbf{K}}{\mathrm{d}\mathbf{b}}\mathbf{z}_{sta}\right) \tag{20}$$

$$\mathbf{M}\frac{\mathrm{d}^2}{\mathrm{d}t^2}\left(\frac{\mathrm{d}\mathbf{z}_{dyn}}{\mathrm{d}\mathbf{b}}\right) + \mathbf{C}\frac{\mathrm{d}}{\mathrm{d}t}\left(\frac{\mathrm{d}\mathbf{z}_{dyn}}{\mathrm{d}\mathbf{b}}\right) + \mathbf{K}\left(\frac{\mathrm{d}\mathbf{z}_{dyn}}{\mathrm{d}\mathbf{b}}\right) = \frac{\mathrm{d}\mathbf{f}_{dyn}}{\mathrm{d}\mathbf{b}} - \frac{\mathrm{d}\mathbf{M}}{\mathrm{d}\mathbf{b}}\ddot{\mathbf{z}}_{dyn} - \frac{\mathrm{d}\mathbf{C}}{\mathrm{d}\mathbf{b}}\dot{\mathbf{z}}_{dyn} - \frac{\mathrm{d}\mathbf{K}}{\mathrm{d}\mathbf{b}}\mathbf{z}_{dyn} \tag{21}$$

The matrices $\mathrm{d}\mathbf{M}/\mathrm{d}\mathbf{b}$, $\mathrm{d}\mathbf{C}/\mathrm{d}\mathbf{b}$ and $\mathrm{d}\mathbf{K}/\mathrm{d}\mathbf{b}$ are the derivatives of system matrices $\mathbf{M}$, $\mathbf{C}$ and $\mathbf{K}$ that include the aero-hydro-elastic contributions, as mentioned earlier. Meanwhile, $\mathrm{d}\mathbf{f}_{sta}/\mathrm{d}\mathbf{b}$ refers to the derivative of static forces, e.g. gravitational and buoyant forces, and $\mathrm{d}\mathbf{f}_{dyn}/\mathrm{d}\mathbf{b}$ is the derivative of external force, e.g. Morison force. Secondly, the design loads (numerator terms) and design resistances (denominator terms) of g_i in Eq. (6)-(16) could be expressed as functions of internal force and geometric variables. The recovery of internal force from system response was carried out using Eq. (22).

$$\mathbf{f}_{internal} = \mathbf{DBz}_{local} \tag{22}$$

where $\mathbf{f}_{internal}$ = internal force vector; $\mathbf{D}$ = constitutive matrix, formed by EA, EI_y and EI_z; $\mathbf{B}$ = strain-displacement matrix; and $\mathbf{z}_{local}$ = local nodal displacement. As a result, g_i is an explicit function of $\mathbf{b}$ and $\mathbf{z}$. The partial derivatives $\partial g_i/\partial \mathbf{b}$ and $\partial g_i/\partial \mathbf{z}$ in Eq. (19) could be evaluated readily.

With regards to the fatigue load constraint, the calculation of ∇g_i was handled differently. The differentiation of Eq. (17) against $\mathbf{b}$ gives Eq. (23). The $\Delta\sigma_{i,HSS}$ here referred to the individual stress range without binning into blocks, while the stress cycle n_i corresponded to either a half or full cycle for the $\Delta\sigma_{i,HSS}$. As such, the $\mathrm{d}n_i/\mathrm{d}\mathbf{b}$ term could be neglected in Eq. (23).

$$\nabla g_{11} = \sum_{i=1}^{I} \frac{mk}{\bar{a}\eta}\left(\frac{1}{t_{ref}}\right)^{mk} t^{mk-1}\frac{\mathrm{d}t}{\mathrm{d}\mathbf{b}} n_i\left(\Delta\sigma_{i,HSS}\right)^{m} + \sum_{i=1}^{I} \frac{m}{\bar{a}\eta}\left(\frac{t}{t_{ref}}\right)^{mk} n_i\left(\Delta\sigma_{i,HSS}\right)^{m-1}\frac{\mathrm{d}\Delta\sigma_{i,HSS}}{\mathrm{d}\mathbf{b}} \tag{23}$$

Among the terms, the derivative of stress range $\mathrm{d}\Delta\sigma_{i,HSS}/\mathrm{d}\mathbf{b}$ was calculated by taking the difference of $\mathrm{d}\sigma_{i,HSS}/\mathrm{d}\mathbf{b}$ at $t_j = t_1$ and $t_j = t_2$, where t_1 and t_2 are the time of initial and half cycle turning points, respectively; which could be identified during the rainflow counting process.

$$\frac{\mathrm{d}\Delta\sigma_{i,HSS}}{\mathrm{d}\mathbf{b}} = \begin{cases} \left.\dfrac{\mathrm{d}\sigma_{i,HSS}}{\mathrm{d}\mathbf{b}}\right|_{t_j=t_1} - \left.\dfrac{\mathrm{d}\sigma_{i,HSS}}{\mathrm{d}\mathbf{b}}\right|_{t_j=t_2} & \text{for } \sigma_{i,HSS}(t_1) > \sigma_{i,HSS}(t_2) \\ \left.\dfrac{\mathrm{d}\sigma_{i,HSS}}{\mathrm{d}\mathbf{b}}\right|_{t_j=t_2} - \left.\dfrac{\mathrm{d}\sigma_{i,HSS}}{\mathrm{d}\mathbf{b}}\right|_{t_j=t_1} & \text{for } \sigma_{i,HSS}(t_2) > \sigma_{i,HSS}(t_1) \end{cases} \tag{24}$$

Meanwhile, the derivative of HSS $\mathrm{d}\sigma_{i,HSS}/\mathrm{d}\mathbf{b}$ was determined from Eq. (25). The constants c_{Nx}, c_{My} and c_{Mz} may vary depending on the HSS locations [11]. Since the SCFs are generally governed by the joint dimensions, the derivatives $\mathrm{d}SCF_i/\mathrm{d}\mathbf{b}$ could be calculated using direct differentiation method. Whereas for the nominal stresses, the derivatives $\mathrm{d}\sigma_i/\mathrm{d}\mathbf{b}$ could be evaluated using the same method as discussed for the extreme load constraints.

$$\begin{aligned}\frac{\mathrm{d}\sigma_{i,HSS}}{\mathrm{d}\mathbf{b}} = {} & c_{Nx}\left(\frac{\mathrm{d}SCF_{Nx}}{\mathrm{d}\mathbf{b}}\sigma_{i,Nx} + \frac{\mathrm{d}\sigma_{i,Nx}}{\mathrm{d}\mathbf{b}}SCF_{Nx}\right) + c_{My}\left(\frac{\mathrm{d}SCF_{My}}{\mathrm{d}\mathbf{b}}\sigma_{i,My} + \frac{\mathrm{d}\sigma_{i,My}}{\mathrm{d}\mathbf{b}}SCF_{My}\right) + \\ & c_{Mz}\left(\frac{\mathrm{d}SCF_{Mz}}{\mathrm{d}\mathbf{b}}\sigma_{i,Mz} + \frac{\mathrm{d}\sigma_{i,Mz}}{\mathrm{d}\mathbf{b}}SCF_{Mz}\right)\end{aligned} \tag{25}$$

Lastly, the gradient of eigenfrequency was calculated using Eq. (26) and (27), as derived in [22].

$$\nabla g_3 = \frac{1}{4\pi}\lambda_l^{-0.5}\frac{\partial\lambda_l}{\partial\mathbf{b}} \tag{26}$$

$$\frac{\partial\lambda_l}{\partial\mathbf{b}} = \phi_l^{\mathrm{T}}\left(\frac{\partial\mathbf{K}}{\partial\mathbf{b}} - \lambda_l\frac{\partial\mathbf{M}}{\partial\mathbf{b}}\right)\phi_l \tag{27}$$

where λ_l = eigenvalue of lth mode; ϕ_l = eigenvector of lth mode.

3.5. Optimization Algorithm

The constrained NLP problem was approximated and solved using the Sequential Quadratic Programming (SQP) approach at each iteration. The integrated code implemented the SQP subroutine available from the Matlab optimization toolbox [23]. The SQP reformulates the general problem as QP subproblem and approximates the Hessian matrix (second-order derivative of the Lagrange function) using the modified Broyden-Fletcher-Goldfarb-Shanno (BFGS) formula. This guarantees positive definite Hessian matrices while ensuring the subproblem to be strictly convex. More details about the SQP method can be found in [24,25].

4. Case Study on OC4 Offshore Wind Jacket Substructure

In order to evaluate the performance of the integrated optimization framework, a case study was performed on the offshore wind jacket substructure within the IEA Task 30 OC4 Project. The OWT system consists of the well-known 5 MW horizontal axis three-bladed baseline turbine developed by the National Renewable Energy Laboratory (NREL) and the support structure system that includes a monopile tower, a concrete transition piece and a jacket substructure [16,26]. The overall wind turbine was assumed to be rigidly clamped onto the ground.

4.1. Design Variables

The jacket substructure is a symmetrical four-legged design which comprises four bays of X-braces and a bottom mudbrace at each side, see Fig. 2. The leg members were assumed to be flooded internally, and the jacket was covered with a layer of marine growth of thickness 0.01 mm and density of 1100 kg/m^3 between water depth -2 m and -40 m. In total, there are 64 tubular joints (24 K-joints, 16 X-joints, and 24 Y- or T-joints).

The design variables selected for this study were the diameters and thicknesses of the jacket members. They were distinct for various bays and member types, either legs or braces. There were 22 design variables in total, where the odd and even numbered design variables represented the member diameters and thicknesses, respectively. In addition, the bottom-most section of the legs was the pile members that protruded out from the soil. They were not included in the optimization study. The initial values of the design variable were based on the OC4 jacket dimensions, as summarized in Fig. 2; whereas the upper and lower bounds were set to be 300 % and 33 % of the initial values, respectively. Furthermore, the D_n/t_n ratios were assigned to be between 20 and 120 for the braces, and between 20 and 64 for the legs. The D_{brace}/D_{leg} and t_{brace}/t_{leg} ratios were constrained between 0.2 and 1.0 [10,11].

4.2. Design Load Cases

The OWT model was subject to combined wind and wave loads in the simulations. The wind and wave conditions were modelled as three-dimensional turbulent wind field according to von Kaimal spectral model, and as Wheeler stretched irregular waves according to the JONSWAP wave spectrum, respectively. The wind parameters, such as mean wind speed at hub height V_{hub}, turbulence intensity (ratio of standard deviation to mean wind speed) TI, wind gradient exponent α, as well as the wave parameters, such as significant wave height H_s, peak spectral period T_p and peak shape parameter γ are summarized in Table 1. The FLS load analysis modelled the operating power production condition under normal turbulent wind (NTM) and normal sea state (NSS); while the turbine was modelled in idling condition under the extreme wind (EWM) and extreme sea state (ESS) for the ULS load case.

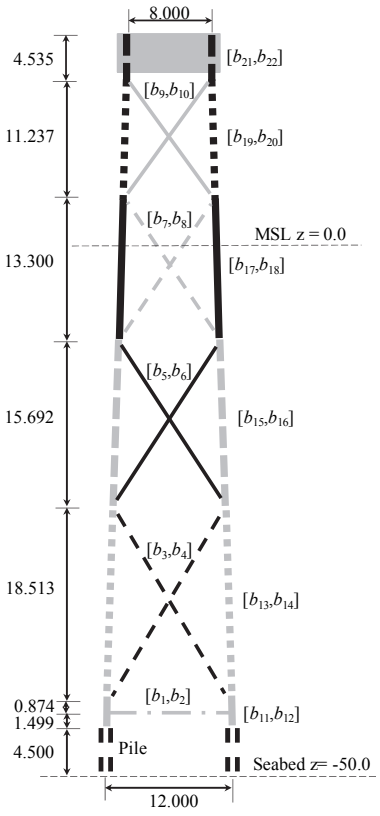

Design Variables	Outer Diameter [m]	Thickness [m]
$[b_1,b_2]$	0.80	0.020
$[b_3,b_4]$	0.80	0.020
$[b_5,b_6]$	0.80	0.020
$[b_7,b_8]$	0.80	0.020
$[b_9,b_{10}]$	0.80	0.020
$[b_{11},b_{12}]$	1.20	0.050
$[b_{13},b_{14}]$	1.20	0.050
$[b_{15},b_{16}]$	1.20	0.035
$[b_{17},b_{18}]$	1.20	0.035
$[b_{19},b_{20}]$	1.20	0.035
$[b_{21},b_{22}]$	1.20	0.040

Fig 2. The OC4 offshore jacket substructure and the initial member dimensions (units are in m)

Table 1. Description of simplified load cases used in the case study

Load Case	Wind Conditions	Wave Conditions
FLS	NTM (Kaimal spectrum)	NSS (JONSWAP spectrum)
	V_{hub} = 8.00 m/s	H_s = 1.31 m
	TI = 10.00 %	T_p = 5.67 s
	α = 0.14	γ = 1
ULS	EWM (Kaimal spectrum)	ESS (JONSWAP spectrum)
	V_{hub} = 42.73 m/s	H_s = 9.40 m
	TI = 10.00 %	T_p = 13.70 s
	α = 0.11	γ = 3.3

5. Results and Discussion

5.1. Accuracy of Sensitivity Analysis

Table 2 summarizes the normalized root-mean-square deviations (NRMSD) of the design sensitivities calculated using DDM and finite difference methods (forward and central difference). The derivatives were evaluated at the initial jacket dimension against brace diameter b_3, brace thickness b_4, chord diameter b_{15} and chord thickness b_{16}, while numerical integrations were carried out with time steps of 0.01 s and 0.025 s, respectively.

The results show that the central difference method attained a very good agreement with DDM in estimating the displacement derivatives for both ULS and FLS load cases, which were generally less than 2.5 percent NRMSD; whereas the forward difference scheme yielded higher discrepancies of up to 6 percent. The forward difference method experienced larger truncation error in comparison with the central difference scheme, when using the same step size in the sensitivity analysis. The deviations become more prominent when considering the nodal displacements of the entire OWT system, reaching a NRMSD of 12 percent. These large deviations occurred at the vertical displacement fields (z-axis) of the structure when varying the jacket leg dimensions. The truncation error accumulated upwards to the other structural parts, e.g. transition piece, tower and nacelle, causing large discrepancies. Similar trends could be observed in the eigenfrequency constraint derivatives when comparing the finite difference methods. The central difference approximation generally performed better than the forward difference scheme, with much smaller NRMSD, except for $\mathrm{d}g_3/\mathrm{d}b_4$.

As for the sensitivities of the extreme load constraints in tubular beams, the NRMSD were generally larger than the other constraint derivatives. The NRMSD reached as high as 22.4 percent, when using the forward difference approximation with a 0.025 s time step. Upon investigation, it was found that these huge deviations took place at beams which experienced alternating tension and compression modes in the sectional normal force or stress. The usage of different formulae between tension and compression modes caused the ULS state functions to be discontinuous at these time steps. The discontinuity resulted in numerical errors when performing the finite difference calculation, due to the mismatches of ULS values at these affected time steps. In some cases, the discrepancy could be eliminated either when a smaller time step was utilized, or when the central difference method, with higher order of accuracy, was used, or both, since these methods might remove the mismatches.

Regarding the extreme load constraints in tubular joints, the derivatives tallied well between DDM and central difference method, giving a NRMSD of below 2.5 percent. When employing the forward difference method in estimating the sensitivities against leg dimensions, the NRMSD were found to be relatively large and the results seemed to correlate with the corresponding displacement sensitivities under the ULS load case. Since the interaction equation applied the same formula for both axial tension and compression modes, it avoided the discontinuity problem. Finally, the comparison between analytical derivatives and central difference approximation for fatigue load constraint produced satisfying NRMSD results that were well below 5 percent. The correlation between results and displacement sensitivities under the FLS load case was not distinct, since the sensitivity analysis is more complicated and involves contributions from other derivatives, such as SCF derivatives.

Table 2. Summary of NRMSD of the sensitivities computed using DDM and finite difference methods

Derivatives	Time step (method)	dg_i/db_3 [%]	dg_i/db_4 [%]	dg_i/db_{15} [%]	dg_i/db_{16} [%]
Displacement under ULS load case	Δt = 0.025 s Forward	2.6434 (2.4550)	2.8410 (2.3894)	5.9049 (7.4122)	5.7200 (6.7929)
	Δt = 0.025 s Central	2.1739 (1.8216)	2.4132 (2.0031)	1.0407 (1.1598)	0.9079 (0.9712)
	Δt = 0.010 s Forward	1.4582 (1.4695)	1.5102 (1.3090)	5.3705 (6.8260)	5.2418 (6.3035)
	Δt = 0.010 s Central	0.8757 (0.7349)	0.9719 (0.8085)	0.4860 (0.5387)	0.4042 (0.4340)
Displacement under FLS load case	Δt = 0.025 s Forward	3.6326 (4.3869)	2.9483 (2.7072)	4.3647 (11.918)	4.2949 (8.9243)
	Δt = 0.025 s Central	2.4404 (2.0997)	2.4661 (2.1671)	1.4902 (1.4805)	1.2174 (1.2375)
	Δt = 0.010 s Forward	2.4595 (3.2722)	1.5938 (1.5443)	3.8886 (11.258)	3.9032 (8.4451)
	Δt = 0.010 s Central	0.9634 (0.8360)	0.9721 (0.8638)	0.6113 (0.6695)	0.5030 (0.5441)
Eigenfrequency constraint	Δt = 0.025 s Forward	0.9439	1.0214	2.1064	2.0847
	Δt = 0.025 s Central	0.1463	2.4051	0.0258	0.0362
	Δt = 0.010 s Forward	0.9439	1.0214	2.1064	2.0847
	Δt = 0.010 s Central	0.1463	2.4051	0.0258	0.0362
Extreme load constraint (beam)	Δt = 0.025 s Forward	18.4280	22.3923	7.5369	8.4559
	Δt = 0.025 s Central	17.9255	1.5763	7.5181	8.4446
	Δt = 0.010 s Forward	18.2616	1.7916	7.4631	8.3772
	Δt = 0.010 s Central	0.7792	1.0068	7.3310	8.2352
Extreme load constraint (joint)	Δt = 0.025 s Forward	3.9071	2.3724	6.1640	7.3502
	Δt = 0.025 s Central	0.8636	0.9225	2.0554	2.1116
	Δt = 0.010 s Forward	3.5686	2.3008	4.7684	6.2169
	Δt = 0.010 s Central	0.4399	0.3299	2.2352	2.3758
Fatigue load constraint	Δt = 0.025 s Forward	6.9605	1.6801	2.7034	1.9704
	Δt = 0.025 s Central	4.5504	1.9618	1.8839	0.8800
	Δt = 0.010 s Forward	4.8361	2.0250	2.3996	1.8080
	Δt = 0.010 s Central	3.8099	1.4374	1.6962	0.5633

Note: Values in parentheses are the NRMSD of derivatives for the overall OWT system.

In general, a smaller time step Δt used in the numerical integration was found to diminish the numerical errors in the sensitivities estimation for both finite difference schemes. Additionally, the accuracy of the finite difference method also depends on the step size Δb used in the sensitivity analysis. The two main sources of errors, i.e. truncation error and condition error, are positively and inversely proportional to Δb, respectively. The optimal step size could be determined from further analysis to minimize the total numerical error, yet this would introduce additional computational burden [27].

In this study, the DDM and central difference method were shown to give comparable results in calculating the derivatives. The forward difference method, on the contrary was not recommended due to the large discrepancy in estimating the sensitivities. Furthermore, the DDM method was twice as efficient in the calculation process, since only $N_{var}+1$ number of system analysis were required instead of $2*N_{var}+1$ for central difference method, for every function and gradient evaluation, where N_{var} is the number of design variables.

5.2. Performance of Integrated Optimization Method

This section discusses the performance of the integrated optimization framework. In the optimization process, the tolerances of step size, first order optimality measure and constraint function were set to be 1E-6, 1E-6 and 1E-2, respectively.

Fig. 2(a) depicts how the optimal support structure mass and the corresponding maximum constraint violations change during the optimization process. The active FLS constraint violations ascended sharply in the beginning of the process, which were in line with the significant mass reduction caused by the decreasing member dimension in general; and progressively fell back to the limits in later iterations as the structural design approached the optimal design. The final jacket design attained a mass reduction of 52 percent as compared with the initial design.

The details about eigenfrequency, extreme load and fatigue load constraints are displayed in Figs. 2(b), (c) and (d), respectively. The first mode side-to-side and foreaft eigenfrequencies varied in a similar pattern as the structural mass, indicating that the lighter support structure was corresponding to the 'softer' design while maintaining the structural integrity against the limit states. Throughout the process, the eigenfrequencies fluctuated within the allowable limits, and finally converged to 0.27 Hz, which was at the center of the constraint limits.

Although the design of bottom fixed jacket substructure is generally fatigue driven, Fig. 2(c) shows that the ULS criteria are as important in governing the design process. In this optimization study, there were 1352 extreme load constraints in total, of which 1248 were contributed from the tubular beams (i.e. 6 constraints g_4 - g_9 for both ends of each beam) and 104 from the tubular joints (i.e. 2 constraints for each X- and K- joints and 1 constraint for each Y-joint). Among the list of ULS criteria implemented, buckling and compression state functions, g_5 and g_6 were found to be active during the optimization process. The former remained as active constraint along with the FLS design constraint at the final iterations, while the structure was gradually tuned to be less fatigue prone. The remaining extreme load constraints were found to be inactive throughout the optimization study. The tensile state function g_4 and extreme load constraint for tubular joints g_{10} were relatively more 'active' in fluctuating within the allowable limit. On the contrary, the variation of g_8 and g_9 constraints were very small at all iterations; due to the minimal shear force and torsional moment experienced

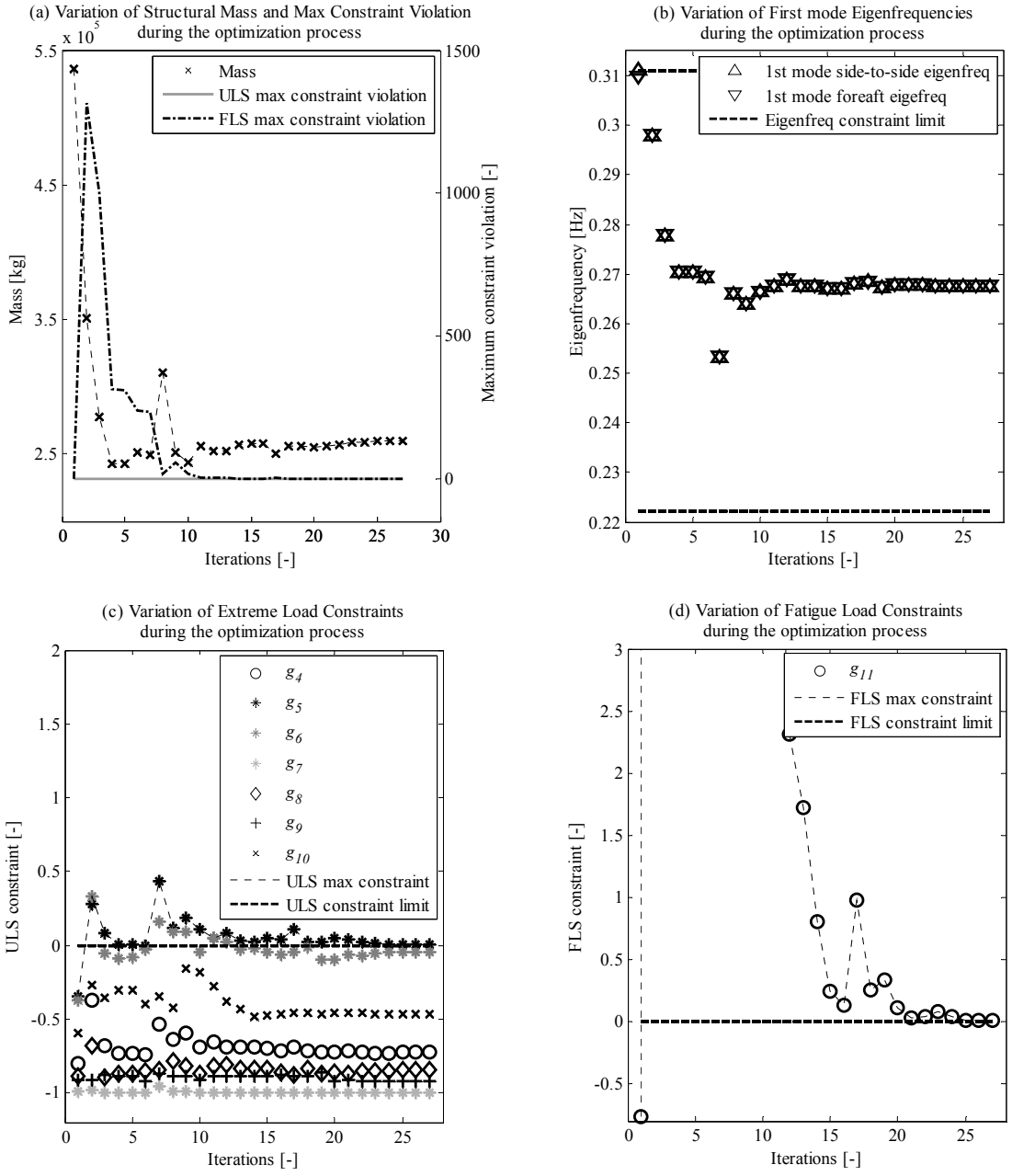

Fig.3 Variation of design objective and constraint functions during the optimization iterations

in tubular members as well as the diameters of jacket members are relatively small for hoop buckling to occur. In addition, g_7 is a conditional design constraint, and it was not activated in most of the iterations.

Fig. 2(d) illustrates the fatigue load constraints change with respect to the optimization iterations. There were 208 constraints imposed in total, with 2 from each end of the members. In general, the g_{11} constraint enveloped the overall design constraints at all iterations. It was the final constraint to converge in the optimization procedure and it governed the feasibility of the optimal solution. Successful local minimal design solution was finally attained when both first order optimality measure and maximum constraint violation were less than the respective tolerance values.

The proposed gradient based optimization method has demonstrated that the NLP design problem of offshore wind turbine support structure could be solved in 27 iterations, indicating a fast convergence in search for an improved design. Since the problem is nonconvex, the global optimum of the solution cannot be guaranteed. One way to carry on with the global optimization is by performing multiple starts at different initial design variables. In addition, this current study used a simplified load case in lieu of the comprehensive design load cases. A detailed optimization of jacket substructure could be extended readily using the same framework.

6. Conclusions

This report gave an overview on the optimal design problem of offshore wind support structure system and presented an analytical gradient-based optimization framework to solve the dynamic constrained optimization problem. Several key features and successful implementation details were:

- The optimization framework carried out the dynamic analysis in time domain, while including a comprehensive list of limit state functions (Sizing, Eigenfrequency, ULS and FLS) as required by the design standards.
- The sensitivity analysis was carried out using the analytical Direct Differentiation Method (DDM). The report discussed and showed the methods how to calculate sensitivities for various design constraints.

In addition, the optimization framework was evaluated in a case study using the OC4 offshore jacket substructure model. The key findings were:

- In the sensitivity analysis, the central difference approximation matched very well with the analytical DDM, yielding NRMSD of less than 5 percent in general. The DDM was also capable of avoiding potential numerical errors occurring during the calculation of the extreme load constraint gradient for tubular beams. The numerical error was due to the discontinuity of ULS utilization factors when the beams were experiencing internal forces/ stresses switching between tension and compression modes.
- The DDM method is comparably more efficient than the finite difference methods since it requires less number of equations to be solved during the optimization process for the similar or better level of accuracy.
- The overall optimization framework demonstrated a successful search for an improved design solution which saved up to 52 percent of structural mass, while satisfying all the design constraints. The procedure was completed in 27 iterations.
- Both fatigue and extreme load constraints exhibited important influences in determining the optimal solution during the optimization process. The FLS constraint was the critical constraint which decided the final optimal design solution. As for the ULS constraints, buckling and compressive load constraints were active during the optimization process while the rest were well below the constraint limit.

Acknowledgements

The authors would like to thank the Singapore Economic Development Board (EDB) - DNV GL - Energy Research Institute @ NTU (ERI@N) Joint Industry Ph.D. Program. Support from the Norwegian Research Centre for Offshore Wind Technology (NOWITECH FME, The Research Council of Norway, project no. 193823) is gratefully acknowledged.

References

[1] The Carbon Trust. *Offshore Wind Power: Big Challenge, Big Opportunity - Maximising the Environmental, Economic and Security Benefits*. Tech. Rep. CTC743, The Carbon Trust; 2008, 112 pp.

[2] Haghi R, Ashuri T, van der Valk PLC, Molenaar DP. Integrated Multidisciplinary Constrained Optimization of Offshore Support Structures. J Phys Conf Series 2014, to appear.

[3] Chew KH, Ng EYK, Tai K, Muskulus M, Zwick D. Offshore Wind Turbine Jacket Substructure: A Comparison Study between Four-Legged and Three-Legged Designs. J Ocean Wind Energy 2014;1(2):74-81.

[4] Zwick D, Muskulus M, Moe G. Iterative Optimization Approach for the Design of Full-Height Lattice Towers for Offshore Wind Turbines. Energy Procedia 2012;24:297-304.

[5] Fylling I, Berthelsen PA. WINDOPT- An Optimization Tool for Floating Support Structures for Deep Water Wind Turbines. Proc 30th Int Conf Ocean Offshore Arct Eng, Rotterdam, The Netherlands, 2011;5:499851:1-10.

[6] Muskulus M, Schafhirt S. Design Optimization of Wind Turbine Support Structures - A Review. J Ocean Wind Energy 2014;1(1):12-22.

[7] IEC. Wind Turbines - Part 3: Design Requirements for Offshore Wind Turbines. International Standard IEC 61400:3, Int Electrotechnical Commission, Geneva, Switzerland; 2009, 263 pp.

[8] Tortorelli DA, Panagiotis M. Design Sensitivity Analysis: Overview and Review. Inverse Probl Eng 1994;1:71-105.

[9] Park GJ. Analytic Methods for Design Practice. Berlin: Springer; 2007, 627 pp.

[10] Standards Norway. NORSOK Standard N-004: Design of Steel Structures, Rev 3. Lysaker, Norway; 2013, 264 pp.

[11] DNV. Fatigue Design of Offshore Steel Structures. Recommended Practice DNV- RP-C203, Det Norske Veritas AS, Høvik, Norway; 2012, 178 pp.

[12] Van der Tempel J, Molenaar D. Wind Turbine Structural Dynamics - A Review of the Principles for Modern Power Generation, Onshore and Offshore. Wind Engineering 2002;26(4):211-20.

[13] Fischer T, de Vries W, Schmidt B. Upwind WP4 Design Basis. Tech. Rep. UpWind, Universität Stuttgart, Stuttgart, Germany; 2010, 140 pp.

[14] ASTM. Standard Practices for Cycle Counting in Fatigue Analysis. ASTM E1049-85, American Society of Testing Materials, West Conshohocken, USA; 2011. 10 pp.

[15] Ong MC, Bachynski EE, Okland OD, Passano E. Dynamic Response of a Jacket Type Offshore Wind Turbine using Decoupled and Coupled Models. Proc of 33rd Int Conf Ocean Offshore Arct Eng, San Francisco, USA, 2014:24246:1-10.

[16] Jonkman J, Butterfield S, Musial W, Scott G. Definition of a 5 MW Reference Wind Turbine for Offshore System Development. Tech. Rep. NREL/TP-500-38060, National Renewable Energy Laboratory, Golden, CO; 2009, 63 pp.

[17] Chopra AK. Dynamics of Structures, 3rd Ed. New Jersey: Prentice Hall; 2006, 876 pp.

[18] Laino DJ, Hansen AC. User's Guide to the Wind Turbine Dynamics Aerodynamics Computer Software AeroDyn. Tech. Rep. prepared for the NREL under Subcontract No. TCX-9-29209-01, Windward Engineering, Salt Lake City, UT; 2002, 54 pp.

[19] Schafhirt M and Muskulus M. Aerodynamic Damping of Wind Turbines under Constant and Turbulent Wind. *Proc 10th PhD Seminar on Wind Energy in Europe,* Orleans, France, 2014:80-83.

[20] Salzmann D, van Der Tempel J. Aerodynamic Damping in the Design of Support Structures for Offshore Wind Turbines. Proc Offshore Wind Energy Conf, Copenhagen, Denmark, 2005:1-9.

[21] Choi KK, Kim NH. Structural Sensitivity Analysis and Optimization 1 - Linear Systems. New York: Springer; 2005, 446 pp.

[22] Fox RL, Kapoor MP. Rates of Change of Eigenvalues and Eigenvectors. AIAA Journal 1968;6(12):2426-29.

[23] Coleman T, Branch MA, Grace A. *Optimization Toolbox for Use with MATLAB: User's Guide, 7th Ed.* Math Works, Inc; 2014.

[24] Arora JS. Introduction to Optimum Design, 3rd Ed. Waltham: Academic Press; 2011, 850 pp.

[25] Nocedal J, Wright SJ. Numerical Optimization, 2nd Ed. New York: Springer; 2006, 664 pp.

[26] Vorpahl F, Popko W, Kaufer D. Description of a Basic Model of the "UpWind Reference Jacket" for Code Comparison in the OC4 Project under IEA Wind Annex. Tech. Rep. UpWind, Franhofer IWES, Bremerhaven, Germany; 2011, 14 pp.

[27] Iott T, Haftka R T, Adelman HM. Selecting Step Sizes in Sensitivity Analysis by Finite Differences. Tech. Report TM-86382, NASA, Washington, DC; 1985: 10 pp.

OPTIMIZATION OF OFFSHORE WIND TURBINE SUPPORT STRUCTURES USING ANALYTICAL GRADIENT-BASED METHOD

Technical Report BAT/MB/OW-R01/2015
Offshore Wind Technology Group

18 March 2015

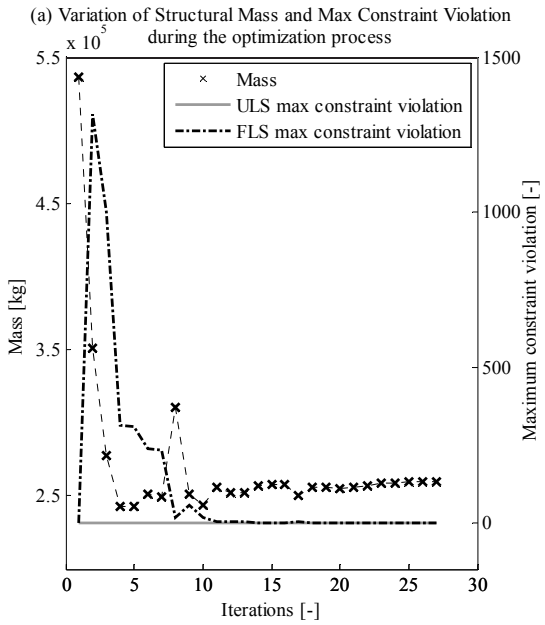

NTNU

ISBN: 978-82-8289-003-8 (paper version)
ISBN: 978-82-8289-004-5 (electronic version)